Electronic Supplementary Information (ESI)

Hierarchical multi-shelled nanoporous mixed copper cobalt phosphide hollow microspheres as a novel advanced electrode for high-performance asymmetric supercapacitors

Seyyed Ebrahim Moosavifard[a*], Saeid Kamari Kaverlavani[b], Javad Shamsi[c] and Ali Bakouei[b]

[a] *Young Researchers and Elite Club, Central Tehran Branch, Islamic Azad University, Tehran, Iran. *Email: info_seyyed@yahoo.com.*

[b] *Department of Physics, Tarbiat Modares University, Tehran, Iran.*

[c] *Nanochemistry Department, Istituto Italiano di Tecnologia, Genova, Italy.*

Experimental details

Synthesis of the multi-shelled nanoporous mixed copper cobalt phosphide hollow microspheres:

The multi-shelled nanoporous mixed copper cobalt phosphide hollow microspheres were synthesized by a facile template free method. In a typical synthesis, 0.0267 mmol of $Cu(NO_3)_2{\cdot}6H_2O$ and 0.0533 mmol of $Co(NO_3)_2{\cdot}6H_2O$ and 0.08 mmol of isophthalic acid (H_2IPA) were added to a mixture of 5 mL DMF and 5 mL acetone under stirring to obtain a homogeneous apparent solution. After 6 h stirring, the result clear solution was transferred into a sealed Teflon-lined stainless-steel autoclave and maintained at 160 °C for 4 h. After cooling down to room temperature, the as-synthesized precursors were separated by centrifugation, followed by annealing at 500 °C in air for 10 min with a heating rate of 5 °C min^{-1}. After then, in order to obtain the multi-shelled nanoporous mixed copper cobalt phosphide hollow microspheres, 10 mg of obtained precursor was annealed at 350 °C in the vicinity of 100 mg sodium hypophosphite monohydrate ($NaH_2PO_2{\cdot}H_2O$) under an Ar flow for 2 h with a heating rate of 5 °C min^{-1}.

Characterization

Structural characterization was performed using X-ray powder diffraction (XRD, Philips X'pert diffractometer with Cu K_α radiation (λ = 0.154 nm). X-ray photoelectron spectroscopy (XPS) analyze was conducted on a VG ESCALAB MKII spectrometer using an Mg K_α X-ray source (1253.6 eV, 120 W) at a constant analyzer. Nitrogen adsorption/desorption, specific surface area and pore size distributions were carried out using a Micromeritics ASAP-2010 apparatus at 77 K by Brunauer–Emmett–Teller (BET) and Barrett–Joyner–Halenda (BJH) methods. The morphologies and structural investigations were done by a TESCAN Mira3 field-emission scanning electron microscope (FESEM) and a Philips transmission electron microscope (TEM).

Electrochemical measurements

All electrochemical measurements were performed in aqueous 3 M KOH solution as the electrolyte. The electrodes were prepared by mixing active material, acetylene black, and polyvinylidene fluoride (PVDF) with a mass ratio of 85:10:5. A solution of the mixture in acetone was prepared and coated (Horizon, M. T. D. I., Iran) on nickel foam as the current, and then dried in 120 ◦C for 2 h. In three-electrode cell configuration, the as-prepared electrodes were used as the working electrode, while a saturated calomel electrode (SCE) electrode and a platinum foil were used as the reference and counter electrodes, respectively. In two-electrode cell configuration (asymmetric device), the as-prepared MN-CCP and AC electrodes were used as the positive and negative electrodes, respectively. For the preparation of the AC electrode, a mixture of the AC powder, carbon black and polytetrafluoroethylene (PTFE) in the weight ratio 85:10:5 was pressed onto a nickel foam and dried at 120 °C for 2 h. According to the specific capacitance of AC electrode (175 F g^{-1}), and in order to achieve the maximum operating potential window and performance, the optimal mass ratio between the positive and negative electrodes (m^+/m^-) was calculated to be around 0.18 based on the charge balance theory ($q^+ = q^-$). Accordingly, the mass loading of 2.5 and 14 mg cm^{-2} was chosen for the MN-CCP (positive) and AC (negative) electrodes, respectively. So, the total mass of the two electrode materials was 16.5 mg cm^{-2}.

$$\frac{m_+}{m_-} = \frac{C_- \times \Delta V_-}{C_+ \times \Delta V_+} \quad (1)$$

where C is the specific capacitance (F g^{-1}) of each electrode measured in a three electrode setup, ΔV is the potential window (V), and m is the mass loading (g).

The specific capacitances (C_{sp}), energy densities (ED, Wh kg^{-1}) and power densities (PD, W kg^{-1}) were calculated from the discharge curves using the following equations:

$$C_{sp} = \frac{I\Delta t}{m\Delta V} \quad (2)$$

$$ED = \frac{C_{sp}\Delta V^2}{2} \quad (3)$$

$$PD = \frac{ED}{\Delta t} \quad (4)$$

where I is the discharge current (A), Δt is the discharge time (s), ΔV is the potential window (V), and m is the mass loading (g).

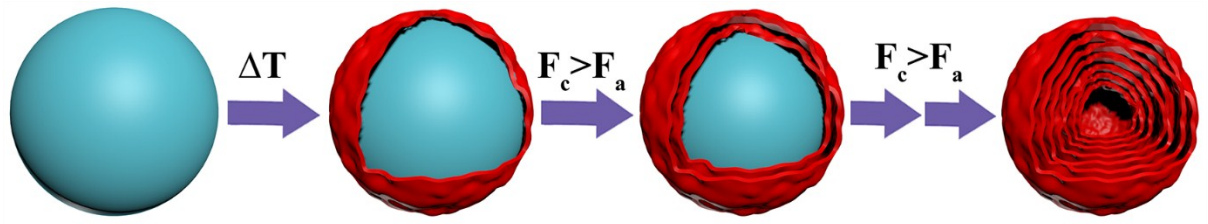

Scheme S1 Schematic illustration of the formation process of multi-shelled nanoporous structure. The multi-shelled structure is formed in a non-equilibrium heat-treatment process. In this process, by applying a large temperature gradient along the radial direction of precursors the first shell is created on the surface of precursors due to surface thermal decomposition of organic components. By creating the first shell, a heterogeneous contraction occurs at the interface layer between the core (cohesive force, F_c) and the shell (adhesive force, F_a). If $F_c > F_a$, the core will be further contracted inward owning to the loss of organic components arising from the continuing heating, and separated from the shell. Because of adhesion force and the residual stress of the phase transformation, the separated shell is crumpled. Upon prolonged annealing, this heterogeneous contraction process continues to take place, and the other shells are formed one after another.[1-3] The porous structure of the shells can be attributed to the decomposition and removal of organic components.[4]

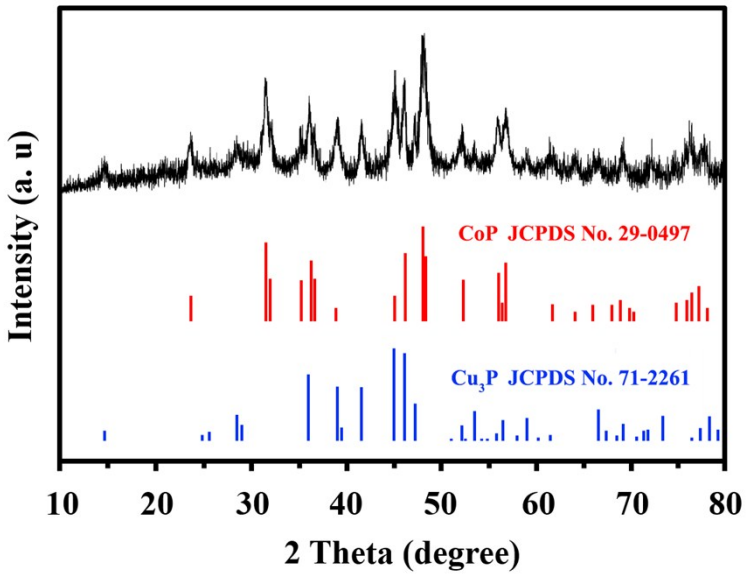

Fig. S1 XRD patterns of MN-CCP sample. As shown, the XRD analysis represents a diffraction peaks which are in good agreement with the orthorhombic phases of CoP (JCPDS No. 29-0497) and the hexagonal phases of Cu_3P (JCPDS No. 71–2261).

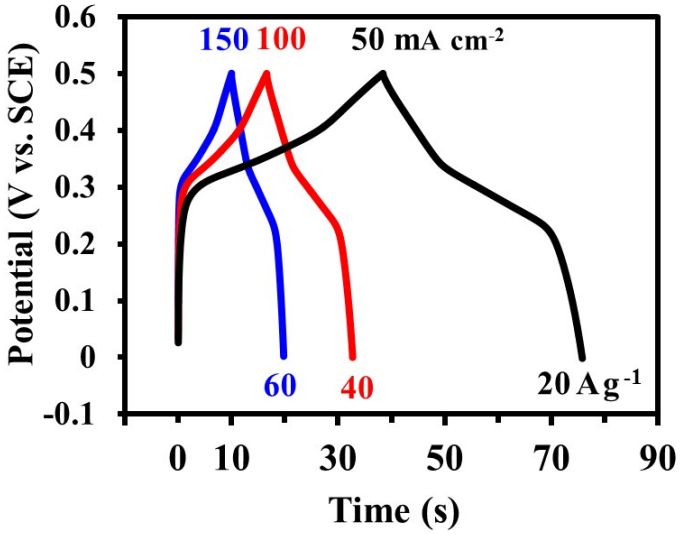

Fig. S2 CD curves of the as-prepared MN-CCP electrode at various current densities.

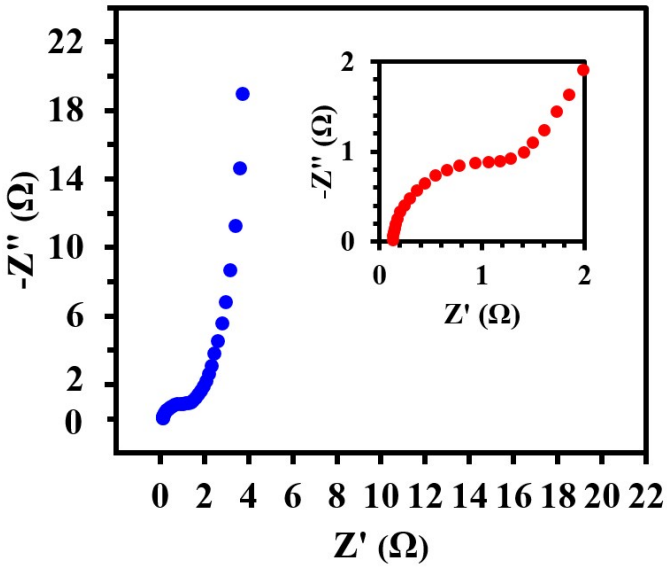

Fig. S3 EIS plot of the MN-CCP electrode. In order to further electrochemical investigation of the as-prepared electrode, EIS experiment was performed. The low internal resistance of the electrode was confirmed from the intercept of the Nyquist curve on the real axis before (0.14 Ω). Furthermore,

the facile pseudocapacitance feature of the electrode was verified by the small charge transfer resistance at high frequencies, and its excellent capacitor characteristics was demonstrated from the linear part observed at low frequencies.

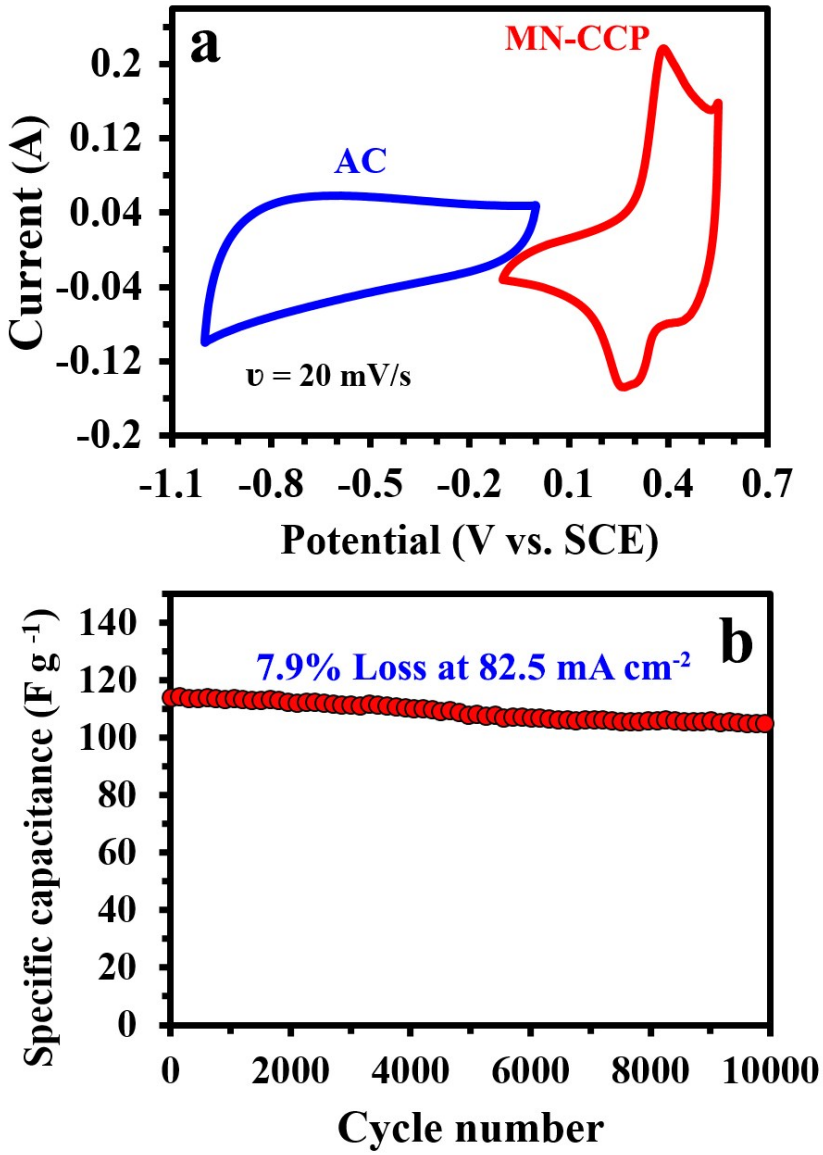

Fig. S4 (a) CV curves of MN-CCP and AC electrodes at a scan rate of 20 mV s^{-1} in a three-electrode system after charge balancing. (b) Long-term cycling stability of the as-prepared MN-CCP//AC asymmetric device over 10000 continuous CDs at a current density of 82.5 mA cm^{-2}.

Table S1. Comparison of the electrochemical performance of MN-CCP electrode in three- and two-electrode systems with other previously reported electrodes.

Morphology/Composition	Capacitance @current density	Cell (Config)	Cycles	Retention	ED (Wh/kg)	Electrolyte	ΔV (V)	Reference (year)
$CuCo_2O_4$ nanostructures	338 F/g at 1 A/g	3E	-	-	-	KOH	0.5	S5 (2014)
$CuCo_2O_4$ nanowires	0.44 F/cm^2 at 1 mA/cm^2	3E	1500	90% at 1 mA/cm^2	-	KOH	0.45	S6 (2015)
	0.47 F/cm^2 at 10 mV/s	2E (vs. AC)	3000	82% at 2 mA/cm^2	-	KOH	1.5	
$CuCo_2O_4$/CuO	57 F/g at 1 mA/cm^2	2E (vs. AC)	5000	79% at 5 mA/cm^2	18	KOH	1.5	S7 (2016)
$CuCo_2O_4$ NSs on graphite	1331 F/g at 1 A/g	3E	5000	80% at 10 A/g	-	KOH	0.6	S8 (2016)
$CuCo_2O_4$ nanobelts	809 F/g at 10 mV/s	3E	1800	127% at 26 mA/cm^2	-	KOH	0.45	S9 (2015)
$CuCo_2O_4$ nanowires	982 F/g at 1.5 A/g	3E	3000	101% at 50 mV/s	-	KOH	0.45	S10 (2017)
	118.5 F/g at 1 A/g	2E (Symm)	2000	82% at 4 A/g	16.9	KOH	1	
Ordered $CuCo_2O_4$	1210 F/g at 1 A/g	3E	-	-	-	KOH	0.5	S11 (2015)
	137 F/g at 1 A/g	2E (vs. AC)	5000	86% at 6 A/g	42.8	KOH	1.5	
$CuCo_2O_4$ @MnO_2 nanoflakes	416 F/g at 1 A/g	3E	4200	92% at 8 A/g	-	Na_2SO_4	1	S12 (2015)
	78 F/g at 1 A/g	2E (vs. AG)	-	-	43.3	Na_2SO_4	2	
$CuCo_2O_4$@$CuCo_2O_4$ nanowire	889 F/g at 2 mA/cm^2	3E	2000	102% at 50 mA/cm^2	-	KOH	0.45	S13 (2017)
	57.6 F/g at 2 mA/cm^2	2E (vs. AC)	2000	101% at 30 mA/cm^2	18	KOH	1.5	
$CuCo_2O_4$ @MnO_2 on carbon fibers	327 F/g at 1.25 A/g	3E	5000	90% at 6.25 A/g	-	KOH	0.5	S14 (2014)
	0.71 F/cm^2 at 1 mA/cm^2	2E (Symm)	-	-	-	PVA/KOH	1	
Double-Sell $CuCo_2O_4$	1472 F/g (2.94 F/cm^2) at 4 mA/cm^2	3E	5000	93.8 % at 10 mA/cm^2	-	KOH	0.5	S15 (2017)
	119 F/g (1.19 F/cm^2) at 20 mA/cm^2	2E (vs. AC)	6000	92.5 % at 50 mA/cm^2	37.3	KOH	1.5	
$CuCo_2O_4$ nanowire @$NiCo_2O_4$ nanosheet	2.6 F/cm^2 at 10 mA/cm^2	3E	4500	80% at 10 mA/cm^2	-	KOH	0.42	S16 (2015)

$CuCo_2O_4$/CuO nanowire	642 F/g at 1 A/g	3E	5000	95% at 8 A/g	-	KOH	0.6	S17 (2016)
	93 F/g at 0.25 A/g	2E (vs.Fe_2O_3)	5000	83% at	33	KOH	1.6	
$CuCo_2O_4$/$MnCo_2O_4$ on graphite paper	1434 F/g at 0.5 A/g	3E	5000	81.4% at 10 A/g	-	KOH	0.5	S18 (2016)
	118.4 F/g at 0.5 A/g	2E	10000	88.4 % at 5 A/g	42.1	KOH	1.6	
$CuCo_2O_4$@$Co(OH)_2$ core/shell	424 F/g at 0.5 A/g	3E	10000	86% at 3 A/g	-	KOH	0.4	S19 (2017)
	70 F/g at 0.5 A/g	2E (vs. AG)	-	-	19.2	KOH	1.4	
$CuCo_2O_4$ nanograsses	796 F/g at 2 A/g	3E	5000	94.7% at 2 A/g	-	KOH	0.6	S20 (2015)
Mesoporous $CuCo_2S_4$	752 F/g at 2 A/g	3E	5000	90% at 3 A/g	-	KOH	0.5	S21 (2016)
Flower-like $CuCo_2S_4$	909 F/g at 5 mA/cm^2	3E	2000	91.1% at 30 mA/cm^2	-	KOH	0.4	S22 (2017)
	93.5 F/g at 1 mA/cm^2	2E (vs. AC)	2000	126% at 25 mA/cm^2	29.2	KOH	1.5	
$CuCo_2S_4$/CNT/graphene	504 F/g at 10 A/g	3E	2000	92.3% at 20 A/g	-	KOH	0.4	S23 (2016)
$FeCo_2O_4$ tube arrays	0.67 F/cm^2 at 2 mA/cm^2	2E (sym)	2000	94% at 4 mA/cm^2	30.9	KOH	1	S24 (2016)
Co_3O_4@Co_3S_4 nanoarrays	1284 F/g at 2 mV/s	3E	5000	93.1% at 4 A/g	-	KOH	0.5	S25 (2016)
	1.28 F/cm3	2E (vs. AC)	6000	90.2% at 20 mA/cm^2	-	PVA-KOH	1.6	
$NiCo_2S_4$@$NiCo_2S_4$ nanosheets	4.38 F/cm^2 at 5 mA/cm^2	3E	5000	82% at 30 mA/cm^2	-	KOH	0.55	S26 (2015)
	75 F/g at 5 mA/cm^2	2E (vs.RGO)	5000	81% at 20 mA/cm^2	24.9	KOH	1.55	
$NiCo_2S_4$@Ni-Mn LDH/GS	1.74 F/cm^2 at 1 mA/cm^2	3E	1000	88.3% at 5 mA/cm^2	-	KOH	0.5	S27 (2015)
	0.5 F/cm^2 at 5 mA/cm^2	2E (vs. VN)	5000	84.5% at 20 mA/cm^2	-	KOH	1.5	
$NiCo_2S_4$@MnO_2 core/shell	2.6 F/cm^2 at 3 mA/cm^2	3E	5000	104% at 50 mV/s	-	KOH	0.55	S28 (2015)
$NiCo_2S_4$@MnO_2 heterostructures	1338 F/g at 2 A/g	3E	2000	82% at 10 A/g	-	KOH	0.45	S29 (2015)
$NiCo_2S_4$@$Ni_3V_2O_8$	512 C/g at 1 A/g	3E	-	-	-	KOH	0.4	S30 (2016)
	150 C/g at 0.5 A/g	2E (vs. AC)	5000	94% at 5 A/g	42.7	KOH	1.6	

$NiCo_2O_4$ nanowires on carbon textile	1283 F/g at 1 A/g	3E	5000	Negligible at 8 A/g	-	KOH	0.4	S31 (2014)
Nickel cobalt oxide nanowires	1479 F/g at 1 A/g	3E	-	-	-	KOH	0.5	S32 (2014)
	105 F/g at 3.6 mA/cm^2	2E(vs. AC)	3000	83 % at 20 mV/s	37.4	KOH	1.6	
Yolk-Shelled $NiGa_2S_4$	2225 F/g at 2 A/g	3E	6000	71% at 20 A/g	-	KOH	0.4	S33 (2017)
	123 F/g at 1.5 A/g	2E (Fe_2O_3)	5000	85% at 12 A/g	43.6	KOH	1.6	
Co_3O_4@PPy@MnO_2 nanowires	629 F/g at 1.2 mA/cm^2	3E	-	-	-	KOH	0.8	S34 (2014)
	96.5 F/g at 0.1 A/g	2E (vs. AC)	10000	100% at 3 A/g	34.3	KOH	1.6	
$ZnCo_2O_4$ nanowire	1625 F/g at 5 A/g	3E	5000	94% at 20 A/g	-	KOH	0.5	S35 (2014)
	0.34 F/cm^2 at 1 mA/cm^2	2E (Symm)	-	-	12.5	KOH	0.8	
$ZnCo_2O_4$ nanoflakes	1220 F/g at 2 A/g	3E	5000	94.2% at 2 A/g	-	KOH	0.6	S36 (2015)
CeO_2@MnO_2 core-shell	255 F/g at 0.25 A/g	3E	3000	90.1% at 2 A/g	-	Na_2SO_4	0.8	S37 (2015)
	49.5 F/g at 0.25 A/g	2E (vs. AGO)	-	-	25.7	Na_2SO_4	2	
$ZnCo_2O_4$@MnO_2 core-shell	2.4 F/cm^2 at 6 mA/cm^2	3E	5000	90% at 24 mA/cm^2	-	KOH	0.5	S38 (2015)
	0.4 F/cm^2 at 2.5 mA/cm^2	2E (Fe_2O_3)	5000	91% at 5 mA/cm^2	37.8	KOH	1.3	
$NiCo_2S_4$ Nanotube on carbon fiber paper	2.86 F/cm^2 at 4 mA/cm^2	3E	2000	96% at 10 mA/cm^2	-	KOH	0.5	S39 (2014)
Zn-Ni-Co ternary oxide	4.2 F/cm^2 at 1.7 mA/cm^2	3E	6000	80.9% at 10 A/g	-	KOH	0.5	S40 (2015)
	114 F/g at 1 A/g	2E (vs. AC)	6000	71.2% at 3 A/g	35.6	KOH	1.5	
$NiCo_2O_4$@$NiMoO_4$ nanowires	1067 F/g at 10 mA/cm^2	3E	5000	84% at 10 mA/cm^2	-	KOH	0.5	S41 (2015)
	-	2E (vs. AC)	5000	87% at 10 mA/cm^2	-	KOH	1.4	
Nickel copper oxide nanowires	2.24 F/cm^2 at 10 mA	3E	1000	90% at 10 A/g	-	KOH	0.5	S42 (2014)
	126 F/g at 2 mA/cm^2	2E (vs. AC)	5000	87% at 20 mA/cm^2	30	KOH	1.3	
Nanoporous CuO	1.5 F/cm^2 at 3.5 mA/cm^2	3E	3000	93% at 7 mA/cm^2	-	KOH	0.5	S43 (2015)
	72.4 F/g at 1 A/g	2E (vs. AC)	3000	96% at 15 mA/cm^2	19.7	KOH	1.4	
Double-shell $NiCo_2S_4$	1263 F/g at 2 A/g	3E	10000	94% at 10 A/g	-	KOH	0.5	S44 (2015)
Mesoporous $NiCo_2S_4$	1440 F/g at 3 A/g	3E	-	-	-	KOH	0.5	S45 (2015)
	90 F/g at 1 A/g	2E (vs. AC)	5000	91.7% at 3 A/g	28.3	KOH	1.5	
Mesoporous Hetero-	749 F/g at 4 A/g	3E	5000	72% at 15 A/g	-	KOH	0.8	S46 (2015)

$NiCo_2S_4/Co_9S_8$	107 F/g at 0.2 A/g	2E (vs. AC)	5000	65% at 5 A/g	33.5	KOH	1.5	
Al@Ni@MnO_x nanospike	942 F/g at 50 mV/s	3E	-	-	-	Na_2SO_4	0.8	S47 (2015)
	59 F/g at 10 mV/s	2E (vs. CCG)	1100	96.3% at 2 A/g	23.02	PVA/Na_2SO_4	1.8	
$NiCo_2S_4$ nano-petals	2036 F/g at 1 A/g	3E	5000	94.3% at 5 A/g	-	KOH	0.4	S48 (2015)
	100 F/g at 1 A/g	2E (vs. AC)	2000	84.2% at 10 A/g	35.6	KOH	1.6	
Carbon fiber paper@ $NiCo_2O_4$ nanowires	680 F/g at 0.5 A/g	3E	-	-	-	NaOH	0.45	S49 (2015)
	97.5 F/g at 1 A/g	2E (vs. GF)	10000	92.2% at 2 A/g	34.5	NaOH	1.6	
Co_2P nanostructures	416 F/g at 1 A/g	3E	-	-	-	KOH	0.7	S50 (2016)
	76.8 F/g at 0.4 A/g	2E (vs. G)	6000	97% at 0.8 A/g	24	KOH	1.5	
Cu_3P nanotube	301 F/g at 2.5 mA/cm^2	3E	-	-	-	H_2SO_4	0.5	S51 (2017)
	143 F/g at 0.75 mA/cm^2	2E (vs. CNT)	5000	81.9% at 10 mA/cm^2	44.6	H_2SO_4	1.5	
Ni-Co-P nanostructures	1448 F/g at 1 A/g	3E	-	-	-	KOH	0.55	S52 (2017)
	64 F/g at 1 A/g	2E (vs. AC)	5000	Negligible at 4 A/g	22.8	KOH	1.6	
Triple-shelled Ni-$Co_{1.5}$-O	1884 F/g at 3 A/g	3E	2000	95.3% at 10 A/g	-	KOH	0.45	S53 (2016)
	132.6 F/g at 1 A/g	2E (vs. rGO)	10000	79.4% at 5 A/g	41.5	KOH	1.5	
NiCoOP@C hybrids	2638 F/g at 1 A/g	3E	3000	84% at 10 A/g	-	KOH	0.5	S54 (2016)
	126.2 F/g at 0.5 A/g	2E (vs. AC)	-	-	39.4	KOH	1.5	
Ni_2P nanosheet	2141 F/g at 50 mV/s	3E	-	-	-	KOH	0.4	S55 (2015)
	96 F/g at 5 mV/s	2E (vs. AC)	5000	91.3% at 1 A/g	26	PVA-KOH	1.4	
MN-CCP	**1946 F/g (4.86 F/cm^2) at 5 mA/cm^2**	**3E**	**6000**	**92.7% at 12.5 mA/cm^2**	**-**	**KOH**	**0.5**	**This work**
	131 F/g (2.16 F/cm^2) at 33 mA/cm^2	**2E (vs. AC)**	**10000**	**92.1% at 82.5 mA/cm^2**	**46.6**	**KOH**	**1.6**	

References

S1. L. Shen, L. Yu, X.-Y. Yu, X. Zhang and X. W. Lou, *Angew. Chem. Int. Ed.*, 2015, **54**, 1868-1872.
S2. B. Y. Guan, A. Kushima, L. Yu, S. Li, J. Li and X. W. D. Lou, *Adv. Mater.*, 2017, **29**, 1605902-n/a.
S3. J. Guan, F. Mou, Z. Sun and W. Shi, *Chem. Commun.*, 2010, **46**, 6605-6607.
S4. Y. V. Kaneti, J. Tang, R. R. Salunkhe, X. Jiang, A. Yu, K. C. Wu and Y. Yamauchi, *Adv. Mater.*, 2017, **29**, 1604898.
S5. A. Pendashteh, M. S. Rahmanifar, R. B. Kaner and M. F. Mousavi, *Chem. Commun.*, 2014, **50**, 1972-1975.
S6. Q. Wang, D. Chen and D. Zhang, *RSC Adv.*, 2015, **5**, 96448-96454.
S7. A. Shanmugavani and R. K. Selvan, *Electrochim. Acta*, 2016, **188**, 852-862.
S8. S. Liu, K. S. Hui and K. N. Hui, *ACS Appl. Mater. Interfaces*, 2016, **8**, 3258-3267.
S9. S. Vijayakumar, S.-H. Lee and K.-S. Ryu, *Electrochim. Acta*, 2015, **182**, 979-986.
S10. L. Liao, H. Zhang, W. Li, X. Huang, Z. Xiao, K. Xu, J. Yang, R. Zou and J. Hu, *J. Alloys Compd.*, 2017, **695**, 3503-3510.
S11. A. Pendashteh, S. E. Moosavifard, M. S. Rahmanifar, Y. Wang, M. F. El-Kady, R. B. Kaner and M. F. Mousavi, *Chem. Mater.*, 2015, **27**, 3919-3926.
S12. M. Kuang, X. Y. Liu, F. Dong and Y. X. Zhang, *J. Mater. Chem. A*, 2015, **3**, 21528-21536.
S13. Y. Zhang, J. Xu, Y. Zheng, Y. Zhang, X. Hu and T. Xu, *RSC Adv.*, 2017, **7**, 3983-3991.
S14. Q. Wang , J. Xu, X. Wang, B. Liu, X. Hou, G. Yu, P. Wang, D. Chen and G. Shen, *ChemElectroChem*, 2014, **1**, 559-564.
S15. S. Kamari Kaverlavani, S. E. Moosavifard and A. Bakouei, *Chem. Commun.*, 2017, **53**, 1052-1055.
S16. K. Zhang, W. Zeng, G. Zhang, S. Hou, F. Wang, T. Wang and H. Duan, *RSC Adv.*, 2015, **5**, 69636-69641.
S17. Y. Wang, C. Shen, L. Niu, R. Li, H. Guo, Y. Shi, C. Li, X. Liu and Y. Gong, *J. Mater. Chem. A*, 2016, **4**, 9977-9985.
S18. S. Liu, K. San Hui, K. N. Hui, J. M. Yun and K. H. Kim, *J. Mater. Chem. A*, 2016, **4**, 8061-8071.
S19. Y. Zhang, H. Liu, M. Huang, J. M. Zhang, W. Zhang, F. Dong and Y. X. Zhang, *ChemElectroChem*, 2017, **4**, 721-727.
S20. J. Cheng, H. Yan, Y. Lu, K. Qiu, X. Hou, J. Xu, L. Han, X. Liu, J.-K. Kim and Y. Luo, *J. Mater. Chem. A*, 2015, **3**, 9769-9776.
S21. Y. Zhu, X. Ji, H. Chen, L. Xi, W. Gong and Y. Liu, *RSC Adv.*, 2016, **6**, 84236-84241.
S22. Y. Zhang, J. Xu, Y. Zhang, Y. Zheng, X. Hu and Z. Liu, *J. Mater. Sci.*, 2017, **52**, 9531–9538.
S23. J. Shen, J. Tang, P. Dong, Z. Zhang, J. Ji, R. Baines and M. Ye, *RSC Adv.*, 2016, **6**, 13456-13460.
S24. B. Zhu, S. Tang, S. Vongehr, H. Xie, J. Zhu and X. Meng, *Chem. Commun.*, 2016, **52**, 2624-2627.
S25. B. Liu, D. Kong, J. Zhang, Y. Wang, T. Chen, C. Cheng and H. Y. Yang, *J. Mater. Chem. A*, 2016, **4**, 3287-3296.
S26. H. Chen, S. Chen, H. Shao, C. Li, M. Fan, D. Chen, G. Tian and K. Shu, *Chem. Asian j.*, 2016, **11**, 248-255.
S27. H. Wan, J. Liu, Y. Ruan, L. Lv, L. Peng, X. Ji, L. Miao and J. Jiang, *ACS. Appl. Mater. Interfaces*, 2015, **7**, 15840-15847.
S28. K. Xu, Q. Ren, Q. Liu, W. Li, R. Zou and J. Hu, *RSC Adv.*, 2015, **5**, 44642-44647.
S29. J. Yang, M. Ma, C. Sun, Y. Zhang, W. Huang and X. Dong, *J. Mater. Chem. A*, 2015, **3**, 1258-1264.
S30. L. Niu, Y. Wang, F. Ruan, C. Shen, S. Shan, M. Xu, Z. Sun, C. Li, X. Liu and Y. Gong, *J. Mater. Chem. A*, 2016, **4**, 5669-5677.
S31. L. Shen, Q. Che, H. Li and X. Zhang, *Adv. Funct. Mater.*, 2014, **24**, 2630-2637.
S32. X. Wang, C. Yan, A. Sumboja and P. S. Lee, *Nano Energy*, 2014, **3**, 119-126.

S33. S. Liu, K. H. Kim, J. M. Yun, A. Kundu, K. V. Sankar, U. M. Patil, C. Ray and S. Chan Jun, *J. Mater. Chem. A*, 2017, **5**, 6292-6298.
S34. L. Han, P. Tang and L. Zhang, *Nano Energy*, 2014, **7**, 42-51.
S35. S. Wang, J. Pu, Y. Tong, Y. Cheng, Y. Gao and Z. Wang, *J. Mater. Chem. A*, 2014, **2**, 5434-5440.
S36. J. Cheng, Y. Lu, K. Qiu, H. Yan, X. Hou, J. Xu, L. Han, X. Liu, J.-K. Kim and Y. Luo, *Phys. Chem. Chem. Phys.*, 2015, **17**, 17016-17022.
S37. S. J. Zhu, J. Q. Jia, T. Wang, D. Zhao, J. Yang, F. Dong, Z. G. Shang and Y. X. Zhang, *Chem. Commun.*, 2015, **51**, 14840-14843.
S38. W. Ma, H. Nan, Z. Gu, B. Geng and X. Zhang, *J. Mater. Chem. A*, 2015, **3**, 5442-5448.
S39. J. Xiao, L. Wan, S. Yang, F. Xiao and S. Wang, *Nano Lett.*, 2014, **14**, 831-838.
S40. C. Wu, J. Cai, Q. Zhang, X. Zhou, Y. Zhu, P. K. Shen and K. Zhang, *ACS Appl. Mater. Interfaces*, 2015, **7**, 26512-26521.
S41. Z. Gu, H. Nan, B. Geng and X. Zhang, *J. Mater. Chem. A*, 2015, **3**, 12069-12075.
S42. L. Zhang, C. Tang and H. Gong, *Nanoscale*, 2014, **6**, 12981-12989.
S43. S. E. Moosavifard, M. F. El-Kady, M. S. Rahmanifar, R. B. Kaner and M. F. Mousavi, *ACS Appl. Mater. Interfaces*, 2015, **7**, 4851-4860.
S44. C. Xia and H. N. Alshareef, *Chem. Mater.*, 2015, **27**, 4661-4668.
S45. Y. Zhu, Z. Wu, M. Jing, X. Yang, W. Song and X. Ji, *J. Power Sources*, 2015, **273**, 584-590.
S46. L. Hou, Y. Shi, S. Zhu, M. Rehan, G. Pang, X. Zhang and C. Yuan, *J. Mater. Chem. A*, 2017, **5**, 133-144.
S47. J. Yang, G. Li, Z. Pan, M. Liu, Y. Hou, Y. Xu, H. Deng, L. Sheng, X. Zhao, Y. Qiu and Y. Zhang, *ACS. Appl. Mater. Interfaces*, 2015, **7**, 22172-22180.
S48. Y. Wen, S. Peng, Z. Wang, J. Hao, T. Qin, S. Lu, J. Zhang, D. He, X. Fan and G. Cao, *J. Mater. Chem. A*, 2017, **5**, 7144-7152.
S49. Q. Tang, M. Chen, L. Wang and G. Wang, *J. Power Sources*, 2015, **273**, 654-662.
S50. X. Chen, M. Cheng, D. Chen and R. Wang, *ACS Appl. Mater. Interfaces*, 2016, **8**, 3892-3900.
S51. Y.-C. Chen, Z.-B. Chen, Y.-G. Lin and Y.-K. Hsu, *ACS Sustain. Chem. Eng.*, 2017, **5**, 3863-3870.
S52. R. Ding, X. Li, W. Shi, Q. Xu and E. Liu, *Chem. Eng. J.*, 2017, **320**, 376-388.
S53. X. Li, L. Wang, J. Shi, N. Du and G. He, *ACS Appl. Mater. Interfaces*, 2016, **8**, 17276-17283.
S54. Y. Shao, Y. Zhao, H. Li and C. Xu, *ACS Appl. Mater. Interfaces*, 2016, **8**, 35368-35376.
S55. K. Zhou, W. Zhou, L. Yang, J. Lu, S. Cheng, W. Mai, Z. Tang, L. Li and S. Chen, *Adv. Funct. Mater.*, 2015, **25**, 7530-7538.